JOURNAL OF GEOPHYSICAL RESEARCH, VOL. 106, NO. B8, PAGES 16,163–16,175, AUGUST 10, 2001

Numerical modeling of magma withdrawal during explosive caldera-forming eruptions

A. Folch and R. Codina

International Center for Numerical Methods in Engineering, Universitat Politècnica Catalunya, Barcelona, Spain

J. Martí

Laboratory of Simulation of Geological Processes, Institute of Earth Sciences "Jaume Almera," Barcelona, Spain

Abstract. We propose a simple physical model to characterize the dynamics of magma withdrawal during the course of caldera-forming eruptions. Simplification involves considering such eruptions as a piston-like system in which the host rock is assumed to subside as a coherent rigid solid. Magma behaves as a Newtonian incompressible fluid below the exsolution level and as a compressible gas-liquid mixture above this level. We consider caldera-forming eruptions within the frame of fluid-structure interaction problems, in which the flow-governing equations are written using an arbitrary Lagrangian-Eulerian (ALE) formulation. We propose a numerical procedure to solve the ALE governing equations in the context of a finite element method. The numerical methodology is based on a staggered algorithm in which the flow and the structural equations are alternatively integrated in time by using separate solvers. The procedure also involves the use of the quasi-Laplacian method to compute the ALE mesh of the fluid and a new conservative remeshing strategy. Despite the fact that we focus the application of the procedure toward modeling caldera-forming eruptions, the numerical procedure is of general applicability. The numerical results have important geological implications in terms of magma chamber dynamics during explosive caldera-forming eruptions. Simulations predict a nearly constant velocity of caldera subsidence that strongly depends on magma viscosity. They also reproduce the characteristic eruption rates of the different phases of an explosive caldera-forming eruption. Numerical results indicate that the formation of vortices beneath the ring fault, which may allow mingling and mixing of parcels of magma initially located at different depths in the chamber, is likely to occur for low-viscosity magmas. Numerical results confirm that exsolution of volatiles is an efficient mechanism to sustain explosive caldera-forming eruptions and to explain the formation of large volumes of ignimbrites.

1. Introduction

Caldera collapse results from the complex coupling between mechanic and thermodynamic processes which control the behavior of the volcanic system and, in particular, that of the associated magma chamber. Field studies reveal that most collapse calderas are related to silicic volcanic systems and form in association with the eruption of large volumes of ignimbrites [*Williams*, 1941; *Smith and Bailey*, 1968; *Lipman*, 1984, 1997]. Moreover, field evidence demonstrates that many explosive caldera-forming eruptions show a preceding central vent Plinian phase that decompresses the magma chamber well below lithostatic pressure, thus giving rise to a caldera phase characterized by the subsidence of the roof of the magma chamber, which causes the extrusion of large volumes of magma through a set of ring faults [*Druitt and Sparks*, 1984; *Martí et al.*, 2000].

The conditions and physical processes leading to explosive caldera-forming eruptions are still not well understood. The magma chamber's mechanical and thermodynamic state immediately before and during caldera collapse has not yet been investigated in detail. Presently, the most detailed information about collapse calderas concerns the distribution and timing of eruption products and the resulting structural collapse [*Williams*, 1941; *Smith and Bailey*, 1968; *Willams and McBirney*, 1979; *Walker*, 1984; *Martí et al.*, 1994; *Branney*, 1995; *Lipman*, 1984, 1997]. From a mechanical point of view, the critical question regarding the formation of collapse calderas concerns the variations in the state of stress required to generate the ring fault system that allows caldera subsidence. Although the stress distribution necessary to generate ring faults can be easily deduced [*Roberts*, 1970; *Gudmundsson*, 1988], the physical conditions leading to that particular stress distribution are still unclear. Decompression of the magma chamber during an opening Plinian phase is insufficient to ensure caldera collapse, as indicated by large historical Plinian eruptions (Vesuvius, El Chichon, and Pinatubo), which did not result in collapse despite significant volumes of magma erupted [*Martí et al.*, 2000]. The occurrence of explosive caldera-forming events depends on the strength of the chamber walls and the depth, water content, and aspect ratio of the magma chamber [*Martí et al.*, 2000]. *Gudmundsson* [1998] and *Gudmundsson et al.* [1997] have proposed that regional loading favors the formation of ring faults. Recently, *McLeod* [1999] has proposed that magmatic buoyancy can also play a major

Paper number 2001JB000181.
0148-0227/01/2001JB000181$09.00

role in attaining the stress conditions necessary for caldera-forming eruptions to occur. The mechanics of collapse calderas and, in particular, the stress conditions and the collapse criteria, require further study in order to provide a comprehensive model for their formation.

The thermodynamic conditions of shallow magma chambers leading to explosive, caldera-forming eruptions are comparatively better constrained [*Druitt and Sparks*, 1984; *Bower and Woods*, 1997; *Folch et al.*, 1998; *Martí et al.*, 2000]. However, the thermodynamic evolution of the magma chamber during a caldera-forming process is still unresolved. The only previous attempt to model such a process numerically is that of *Spera* [1984], who solved the two-dimensional Navier-Stokes equations assuming magma as an incompressible flow and imposing an arbitrary subsidence rate. Other numerical models have addressed the eruption dynamics at the vent during caldera-forming eruptions considering the decompression of the upper part of the chamber [*Wohletz et al.*, 1984].

A more complete approach should involve the coupling between the magma withdrawal process and the behavior of the host rock, thus implying the solution of a fluid-structure interaction problem. The goal of this paper is to develop a numerical procedure to model the temporal evolution of the physical properties of magma during caldera-forming eruptions. The paper does not investigate the causes of caldera-forming eruptions, but builds on previous work investigating the temporal evolution of the physical parameters from the initiation of the Plinian phase to the initiation of caldera collapse [*Folch et al.*, 1998; *Martí et al.*, 2000]. The paper is organized as follows. First, the physical model and the governing equations are introduced. The physical model is based on a simple piston-like rigid block that subsides into a magma chamber. Second, a numerical procedure to solve this fluid-structure interaction problem in the context of a finite element method (FEM) is developed. Finally, numerical examples are given and their geological implications discussed in the light of what is presently known from natural calderas.

2. Physical Model and Governing Equations

Numerical modeling of caldera-forming eruptions can be considered within the general frame of those fluid-structure interaction problems in which a rigid structure moves within the fluid (Figure 1). In such intimately coupled problems, the time-dependent position of a structure (in our case, the block that subsides) determines some boundaries of the fluid (the magma), and, in turn, some properties of the flow such as pressure and stress act as boundary conditions that partially affect the structural dynamics. In the particular case of caldera-forming eruptions, it is obvious that those boundaries of the fluid in contact with the structure (the boundary Γ_{FS}) will undergo large-amplitude motion during the collapse process and, consequently, it will be necessary to consider the numerical solution of the flow-governing equations using a deforming mesh. For this purpose it is convenient to write the flow-governing equations using an arbitrary Lagrangian-Eulerian (ALE) formulation, in which the frame of reference moves with a velocity $\hat{\mathbf{u}}(t)$ with respect to the classical fixed reference frame. The goal of the ALE formulation is to keep all the advantages that the traditional Eulerian description provides in the treatment of fluids while simultaneously incorporating some characteristic aspects of the traditional Lagrangian description such as accuracy in the description of the moving boundaries. As usual [e.g., *Spera*, 1984; *Trial et al.*, 1992], we assume for simplicity that magma is a Newtonian fluid. In consequence, the equations that govern its behavior are the Navier-Stokes equations, which using an ALE formulation are [*Hughes et al.*, 1981],

$$\frac{\partial \rho}{\partial t} = -\nabla \cdot \mathbf{U} + \hat{\mathbf{u}} \cdot \nabla \rho \quad , \tag{1}$$

$$\frac{\partial \mathbf{U}}{\partial t} = -\nabla \cdot (\mathbf{u} \otimes \mathbf{U}) - \nabla p + \nabla \cdot \mathbf{T} + \rho \mathbf{g} + \hat{\mathbf{u}} \cdot \nabla \mathbf{U} \quad , \tag{2}$$

$$\mathbf{T} = \mu \left(\nabla \mathbf{u} + \mathbf{u} \nabla - \frac{2}{3} (\nabla \cdot \mathbf{u}) \mathbf{I} \right) \quad , \tag{3}$$

where (see notation section) t is time, ρ is density, p is pressure, μ is viscosity, $\mathbf{u}$ is the velocity vector, $\mathbf{U} = \rho \mathbf{u}$ is the momentum vector, $\mathbf{g}$ is the acceleration due to gravity, $\hat{\mathbf{u}}$ is the velocity of the ALE dynamic mesh, and $\mathbf{T}$ is the viscous stress tensor (the Cauchy stress tensor without its isotropic pressure term). Equations (1) and (2) are, respectively, the ALE continuity and the ALE momentum equations, derived from general principles of mass and momentum conservation. Note that in the ALE version of these equations a new term that accounts for the relative movement between the frame of reference and the fixed laboratory system appears with respect to the traditional Eulerian formulation. Equation (3) is nothing but the constitutive equation of a Newtonian fluid.

The above set of equations must be complemented with a state law. The state law adopted in the present model is that of *Folch et al.* [1998], deduced assuming the following: (1) Magma is a continuous medium composed by a liquid phase and a single volatile species (H_2O in the case of magmas of silicic compositions and, usually, CO_2 in the case of basic

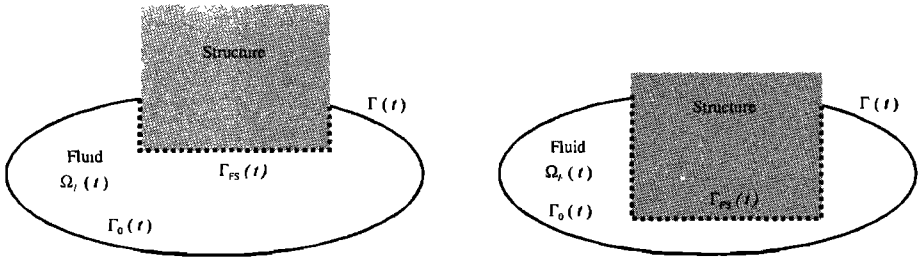

Figure 1. Fluid-structure interaction problem. A structure moves within a fluid consisting of a time-dependent domain $\Omega_F(t)$. The boundary $\Gamma(t)$ of the domain $\Omega_F(t)$ can be decomposed as $\Gamma = \Gamma_{FS} \cup \Gamma_0$ ($\Gamma_{FS} \cap \Gamma_0 = \varnothing$), where $\Gamma_{FS}(t)$ is the time-dependent fluid-structure interface (dashed line).

magmas). (2) The solubility χ of the volatile species is given by Henry's law $\chi = s\,p^m$, where s and m are parameters that depend on both magma and volatile compositions [*Tait et al.*, 1989]. (3) The oversaturation in volatiles and their subsequent exsolution to form gas bubbles take place instantaneously once the ambient pressure equals the critical (exsolution) pressure p_e. (4) If oversaturated in volatiles, magma is a two-phase mixture composed by an incompressible liquid with dispersed bubbles of compressible gas in thermal and mechanical equilibrium, that is, one assumes a bubbly flow regime under the homogeneous approach. Only a single volatile phase is assumed for simplicity. (5) The gas phase behaves as a perfect gas. A discussion on these hypotheses is given by *Folch et al.* [1998].

On the basis of these five assumptions, the state law is given by *Folch et al.* [1998],

$$\rho = \frac{\rho_l}{1 + \left(\frac{\rho_l Q T}{p}\right)\left(\frac{W - s p^m}{1 - s p^m}\right)\Theta(p_e - p)} \quad , \tag{4}$$

where ρ_l is the liquid density, Q is a gas constant (Q=461.66 $J°K^{-1}kg^{-1}$ for water), T is temperature (here assumed constant), W is the volatile mass fraction (including both dissolved and exsolved contributions), and Θ is the step function, defined as $\Theta = 0$ for $p > p_e$ and $\Theta = 1$ for $p \le p_e$. An important feature of state law (4) is that it presents two differentiated domains: Below the exsolution level ($p > p_e$) all the volatiles are dissolved in the liquid and the magma has a constant density $\rho = \rho_l$, while above this level ($p \le p_e$) the liquid is oversaturated in volatiles, the exsolved volatiles forming gas bubbles and magma becoming a two-phase compressible mixture in which density depends nonlinearly on pressure. The homogeneous approach constrains the applicability of the state law to high-viscosity, chemically evolved magmas in the bubbly flow regime [*Papale*, 1996].

The set of equations (1) to (4) must be solved in a time-dependent domain $\Omega_F(t)$ together with a given set of boundary and initial conditions to find density, pressure, and velocity. The fluid domain $\Omega_F(t)$ clearly depends on the dynamics and the rheology of the structure, so that an additional equation must be added to account for the structural response. For simplicity, the model assumes that the block subsides as a rigid solid, whose behavior is governed by Newton's second law,

$$M_b \ddot{\mathbf{d}} = \mathbf{f}^{\mathbf{FS}} + M_b \mathbf{g} \quad , \tag{5}$$

where M_b is the mass of the block, $\mathbf{d}$ is its position (superscript dots indicate temporal derivatives), and $\mathbf{f}^{\mathbf{FS}}$ is the vector of forces that the fluid exerts on the collapsing block, given by

$$\mathbf{f}^{\mathbf{FS}} = \oint_{\Gamma_{FS}} (p\,\mathbf{n} - \boldsymbol{\tau}\cdot\mathbf{n})\, d\Gamma \quad , \tag{6}$$

where $\mathbf{n}$ is the outward unit normal to Γ_{FS}. Clearly, equation (5) is intimately coupled with the Navier-Stokes equations by means of (6), and its solution allows determination of the fluid domain $\Omega_F(t)$ at any time instant. Two constraints must be added to the system. First the flow and the structural equations are intimately coupled by the fact that the velocity field of the structure $\dot{\mathbf{d}}$ and that of the fluid $\mathbf{u}$ must be, at any time instant, compatible at the fluid-structure interface $\Gamma_{FS}(t)$, that is,

$$\dot{\mathbf{d}}(t) = \mathbf{u}(t) \ \text{ on } \Gamma_{FS}(t) \quad . \tag{7}$$

In fact, equation (7) is the ALE version of the classical nonslip condition. On the other hand, the structure and the ALE dynamic mesh are coupled by means of

$$\begin{aligned} \mathbf{d}(t) &= \hat{\mathbf{x}}(t) \\ \dot{\mathbf{d}}(t) &= \hat{\mathbf{u}}(t) \end{aligned} \quad \text{on } \Gamma_{FS}(t) \quad , \tag{8}$$

where $\hat{\mathbf{x}}$ are the time-dependent coordinates of the mesh. The second condition in the above equation is imposed because a discontinuity between the velocities of the structure and the fluid mesh at the fluid-structure interface can perturb the energy exchange.

3. Numerical Method

We propose a general method to solve equations (1) to (5) together with the constraints imposed by (7) and (8). The methodology has been specifically developed to model the behavior of magma chambers during caldera-forming eruptions, but is general and could be applied to any fluid-structure interaction problem where the structure behaves as a rigid solid without rotational degrees of freedom. The numerical procedure is fully developed and tested using standard benchmark problems by *Folch* [2000], and only the general features are outlined in this paper.

3.1. General Procedure

In order to solve the fluid-structure interaction problem, the governing equations for the structure and fluid should be integrated simultaneously. Nevertheless, the solution of this coupled problem via a monolithic scheme is an expensive procedure and presents computational drawbacks, because every component of the coupled problem has its own mathematical and numerical properties as well as its own software implementation requirements. An alternative is to use a partitioned or staggered procedure in which the fluid and the structural equations are alternately integrated in time by using separate solvers. The interaction is then taken into account by means of the boundary conditions. The advantage of the staggered procedure is that it keeps software modularity, simplifies the code, and, for small time step sizes, the solution converges to that of the monolithic scheme. The general procedure for the staggered method is illustrated schematically in Figure 2. Given the fluid-structure states at $t = t^n$, the aim is to find the solution of the coupled system at $t^{n+1} = t^n + \Delta t$, Δt being the time step size under consideration. Each time step of the staggered procedure is as follows: (1) Solve the structural equations to estimate the position of the structure at t^{n+1}, that is, the domain of the fluid $\Omega_F(t^{n+1})$. (2) Transfer the motion of the boundary of the structure to the dynamic mesh of the fluid by imposing the first condition of equation (8) and use the quasi-Laplacian method to compute the configuration of the mesh at t^{n+1}. (3) Check whether there is an unacceptable mesh distortion and, if so, perform remeshing. (4) Determine the mesh velocity $\hat{\mathbf{u}}$ and the boundary conditions for the fluid at the fluid-structure interface Γ_{FS} during the interval (t^n, t^{n+1}) in a manner compatible with the constraints imposed by equations (7) and (8). (5) Solve the equations of the fluid and compute the forces over the structure at t^{n+1} by means of equation (6). These steps are discussed in detail below. Note that, in general, the order of resolution of the staggered procedure (integrate the

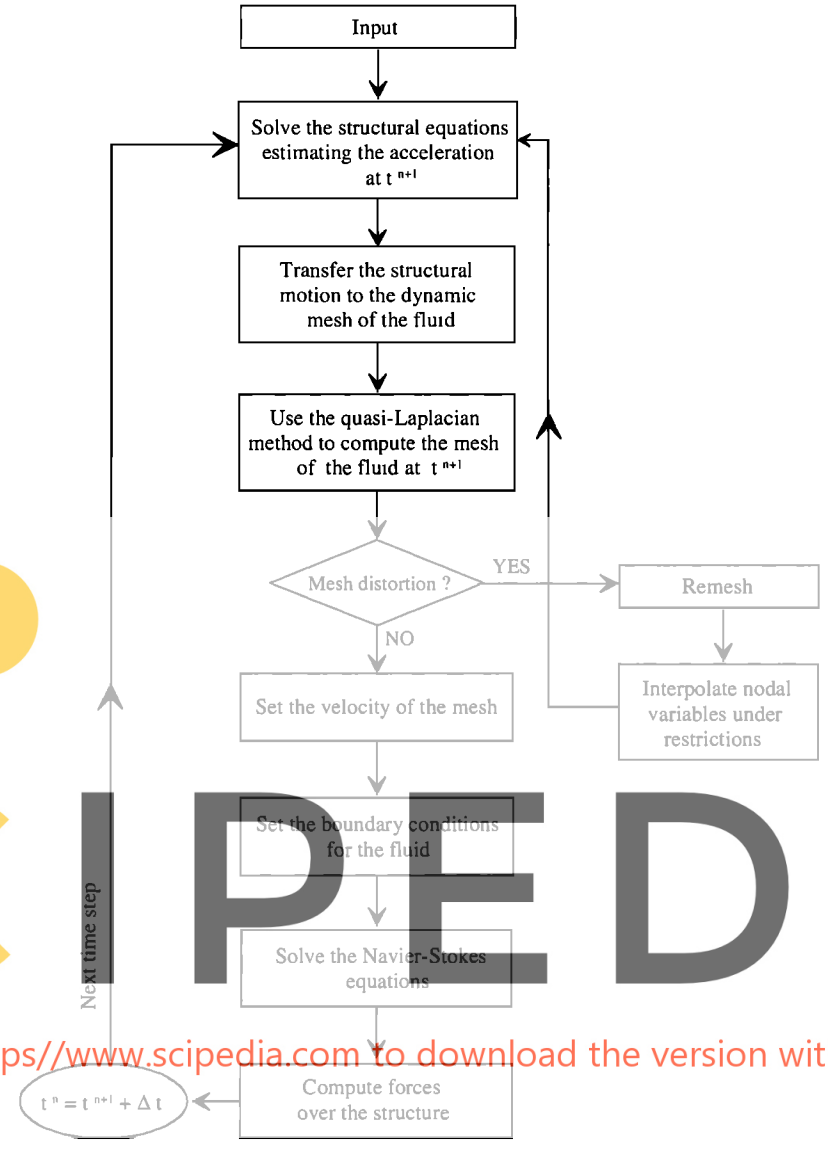

Figure 2. Diagram of the staggered procedure used to solve a certain time step of the fluid-structure interaction problem.

structure first and then the fluid or vice versa) is irrelevant if Δt is small enough. However, for our particular purposes, it is necessary to keep the order indicated above because, at $t=0$, the structure responds to the initial stage of the fluid.

3.2. Solution of the Structural Equations

The structural equations are integrated in time using the constant average acceleration method [*Blom*, 1998]. This method is of order $O(\Delta t^2)$ and constitutes the optimal case of the Newmark method. Let $\mathbf{d}^n$, $\dot{\mathbf{d}}^n$, $\ddot{\mathbf{d}}^n$, and $\ddot{\mathbf{d}}^{n+1}$ be the given position, velocity and accelerations of the structure at times $t=t^n$ and $t=t^{n+1}$, respectively. Then, in the constant averaged acceleration method, the position and the velocity of the structure at $t=t^{n+1}$ are obtained by solving the following system,

$$\begin{bmatrix} \frac{4}{\Delta t^2} I & 0 \\ -\frac{2}{\Delta t} I & I \end{bmatrix} \begin{bmatrix} \mathbf{d}^{n+1} \\ \dot{\mathbf{d}}^{n+1} \end{bmatrix} = \begin{bmatrix} \frac{4}{\Delta t^2} I & \frac{4}{\Delta t} I \\ -\frac{2}{\Delta t} I & -I \end{bmatrix} \begin{bmatrix} \mathbf{d}^n \\ \dot{\mathbf{d}}^n \end{bmatrix} + \begin{bmatrix} \ddot{\mathbf{d}}^{n+1} + \ddot{\mathbf{d}}^n \\ 0 \end{bmatrix} \quad , (9)$$

where I is the identity matrix. It should be noted that the solution of (9) explicitly assumes that $\ddot{\mathbf{d}}^{n+1}$ is known, that is, that the vector of forces $\mathbf{f}^{FS}$ is known at $t=t^{n+1}$. However, in the case of fluid-structure interaction problems, this value is, in general, an unknown at this stage. Therefore it is necessary to do some structural prediction based, for instance, on some extrapolation from previous values of the acceleration. In particular, we have performed a third-order explicit approach using values at t^n, t^{n-1}, and t^{n-2}.

3.3. Quasi-Laplacian Method

Once the position of the structure has been determined at $t=t^{n+1}$ (i.e., once we know the domain of the fluid $\Omega_F(t^{n+1})$), the new coordinates of the dynamic mesh $\hat{\mathbf{x}}$ at this time instant can be computed. This is done using the quasi-Laplacian method, a procedure introduced by *Masud and Hughes* [1997]. The idea is to solve, using a finite element method, the following problem:

$$\begin{aligned} \nabla\cdot\left[(1+\xi)\,\nabla\hat{\mathbf{x}}\right]&=\mathbf{0} \quad \text{in} \quad \Omega_F \\ \hat{\mathbf{x}}&=\mathbf{d} \quad \text{on} \quad \Gamma_{FS} \\ \hat{\mathbf{x}}&=\mathbf{0} \quad \text{on} \quad \Gamma_0 \end{aligned} \quad , \tag{10}$$

where ξ is a bounded, nondimensional function defined for each element of the FEM mesh as

$$\xi^e \equiv \frac{1-A^e_{\min}/A^e_{\max}}{A^e/A^e_{\max}} \quad , \tag{11}$$

and where $A^e_{\min}$ and $A^e_{\max}$ are the minimum and the maximum elemental areas (volumes) of the mesh and A^e is the area (volume) of the element under consideration. This method's main advantage is that it recovers the traditional Laplacian method when the mesh is uniform (when $A^e_{\min}=A^e_{\max}=A^e$, then $\xi^e=0\ \forall e$), whereas for nonuniform meshes the smaller elements translate with less distortion and the larger ones absorb the motion. This prevents element inversion and maintains the shape of elements in refined zones such as boundary layers. The first condition of (8) has been introduced explicitly as a boundary condition when solving (10). The solution of (10) allows the new configuration of the mesh to be determined by adding, as a computational cost, the solution of a linear system of algebraic equations

$$\mathbf{K}\,\mathbf{x}=0 \quad , \tag{12}$$

where $\mathbf{x}$ is the vector of nodal displacements and $\mathbf{K}$ is the matrix arising from the finite element discretization of $\nabla\cdot\left[(1+\xi)\,\nabla\hat{\mathbf{x}}\right]$.

3.4. Mesh Distortion and Remeshing

The solution of equation (10) determines a new configuration for the fluid mesh at every time step. Here, criteria to evaluate mesh distortion are considered. This is achieved by imposing a maximum and a minimum value for the elemental angles of the mesh. Whenever one or more elements of the mesh are unacceptably stretched, a remeshing and subsequent nodal interpolation from the old mesh to the new one are performed. Nodal variables are transmitted using classical Lagrange interpolation functions with some constraints that guarantee global conservation of quantities such as mass, momentum, or forces. This technique [*Houzeaux and Codina*, 2001] allows a compromise between the variable continuity and the global information it carries. The remeshing procedure is undesirable because of the computational cost and inherent projection errors. However, one of the advantages of the ALE formulation with adequate mesh movement is that the remeshing is necessary only rarely, for large structural displacements.

3.5. Mesh Velocity and Boundary Conditions

A key point in fluid-structure interaction is how to integrate the Navier-Stokes equations. Since the spatial configuration changes in time, the choice of appropriate time integration points is crucial. In FEM the normal procedure is first to discretize the equations in time using finite differences and obtain the weak form by integrating over the spatial domain. Thus once the equations are time-discretized, the use of a FEM leads to the evaluation of spatial integrals. This raises the question of where, in the case of time-dependent spatial domains, to evaluate these integrals: on the mesh configuration $(t^n,\hat{\mathbf{x}}^n)$, or on $(t^{n+1},\hat{\mathbf{x}}^{n+1})$, or on a combination. A common procedure is to solve the ALE Navier-Stokes equations considering both $\hat{\mathbf{u}}$ and configuration of the dynamic mesh at $t^{n+1/2}$, by using

$$\hat{\mathbf{u}}^{n+1/2}=\frac{\hat{\mathbf{x}}^{n+1}-\hat{\mathbf{x}}^n}{\Delta t} \quad , \tag{13}$$

and

$$\hat{\mathbf{x}}^{n+1/2}=\frac{\hat{\mathbf{x}}^{n+1}+\hat{\mathbf{x}}^n}{2} \quad . \tag{14}$$

The use of (13) combined with the constant average acceleration method for advancing the structure guarantees that the second constraint of equation (8) is satisfied at a discrete level [*Blom*, 1998]. In general, not all the structural integrators can satisfy this condition of continuity between the velocities of the structure and dynamic mesh at Γ_{FS}. As pointed out by *Farhat et al.* [1995], this justifies the use of this integrator for low-frequency-dominated structural equations (without oscillatory behavior).

Another important issue concerns the prescription of the fluid boundary conditions at the fluid-structure interface, that is, which value of $\mathbf{u}$ must be prescribed at $t^{n+1/2}$ to verify the constraint imposed by equation (7). For the constant average acceleration method the structural velocity $\dot{\mathbf{d}}$ is linear in time so that its value at $t^{n+1/2}$ is given directly by the trapezoidal rule. Therefore if one sets the fluid velocity as

$$\mathbf{u}^{n+1/2}=\frac{1}{2}\left(\dot{\mathbf{d}}^{n+1}+\dot{\mathbf{d}}^n\right) \quad , \tag{15}$$

then the required constraint is satisfied at a discrete level because

$$\mathbf{u}^{n+1/2}=\frac{1}{2}\left(\dot{\mathbf{d}}^{n+1}+\dot{\mathbf{d}}^n\right)=\dot{\mathbf{d}}^{n+1/2} \tag{16}$$

When the no-slip condition is considered, the particles of the structure and the fluid and the nodes of the dynamic mesh coincide at the fluid-structure interface, that is, the ALE formulation becomes Lagrangian at this part of the domain. This is significant because a major goal of the ALE formulation is to provide a Lagrangian description in zones such as moving boundaries of free surfaces.

3.6. The Navier-Stokes Equations

The final step of the staggered procedure involves numerical solution of the ALE Navier-Stokes equations using a FEM. The algorithm uses a fractional step method combined with a pressure gradient projection technique that provides additional stabilization of the pressure field and allows a fully implicit scheme of order $O(\Delta t^2)$. The algorithm can be solved for both compressible and incompressible flows. This is important in simulations of volcanic eruptions because the state law for the magma assumed by the physical model presents two domains: incompressible below the exsolution level and compressible above it. A detailed description of the algorithm has been given by *Folch et al.* [1999] and *Folch* [2000].

4. Numerical Results

Numerous simulations of caldera collapse processes in silicic magmas have been performed using the algorithm

described above. Accuracy of numerical solutions has been checked using different meshes and time step sizes. This section describes the results obtained for a particular numerical simulation that exemplifies features found in the rest of the cases and the applicability of the numerical procedure. Obviously, the quantitative results vary considerably from one simulation to another. However, in general, similar qualitative behavior is observed. Interesting results are obtained, but caution is applied to their geological interpretation since they represent a simplification of the natural system.

An elliptical chamber with major axis a =4 km and minor axis b =0.5 km is located at depth H_{cha} =4 km below the Earth's surface (Figure 3). Recent studies [*Gudmundsson et al.*, 1997; *Gudmundsson*, 1998] investigating stress fields favoring the generation of ring faults suggest that sill-like chambers offer the most suitable stress configuration for the initiation of ring faults. The assumed chamber has an aspect ratio as suggested by these previous studies. Magma flows through a ring fault of thickness r_c =50 m located at a distance a_c =3.5 km from the symmetry axis. The resulting caldera depression has a diameter of 7 km. For simplicity, numerical calculation starts once the ring fault is already open and the caldera-forming eruption has begun. Preceding phases of the eruption in which the chamber is decompressed and the ring faults formed are neglected. An important limitation of the model is that the state law proposed for the magmatic mixture assumes thermal and mechanical equilibrium between liquid and gas phases. This equilibrium is justified as long as the bubbly flow

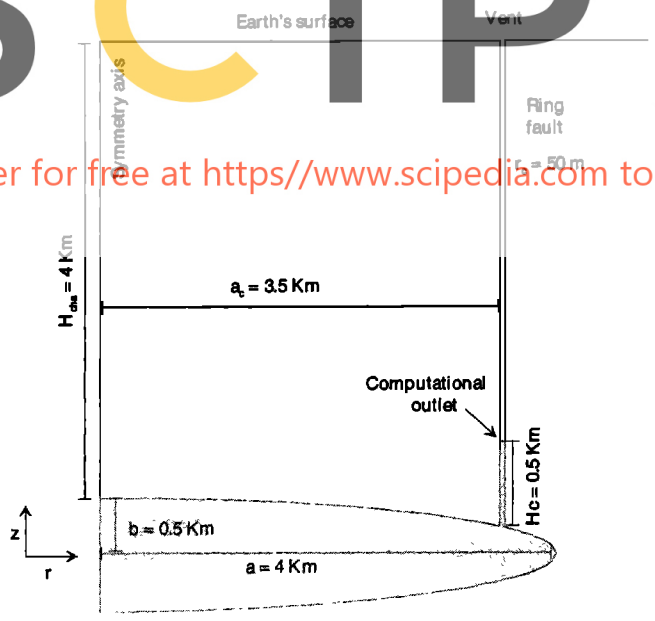

Figure 3. Geometry at the onset of the caldera-forming eruption. The symmetry axis is located at r =0, and the origin of coordinates is at the center of the chamber. An elliptical chamber with major axis a =4 km and minor axis b =0.5 km is located at depth H_{cha} =4 km below the surface of the Earth. Magma flows through a ring fault of thickness r_c =50 m located at a distance a_c =3.5 km from the symmetry axis. The diameter of the resulting collapse caldera is 7 km. The conduit is cut at a distance H_c =0.5 km in order to ensure the validity of the state law, so that the computational outlet does not coincide with the physical one (the vent). The computational domain for the fluid is shaded.

regime is sustained and becomes unrealistic in the uppermost parts of the conduit, near and above the fragmentation level [*Folch et al.*, 1998]. To satisfy this condition, the conduit is cut at a distance H_c =0.5 km so that the computational outlet does not coincide with the physical vent. An adequate physical treatment of this region would require the solution of a nonhomogeneous problem, where governing equations for liquid and gas phases are considered separately.

The geometry has been discretized using meshes with linear triangular elements. A mesh is considered to become unacceptable when none of its elements has an angle lower than 10° or greater than 160°. When this critical condition is attained, a new mesh is generated, and the nodal variables are interpolated onto the new mesh. Although in this simulation large structural displacements and thus large mesh deformations are involved, only six different meshes are required to simulate the collapse process. General and detailed views the first and the last of these meshes are shown in Figure 4.

Boundary and initial conditions of the model are illustrated in Figure 5. The no-slip condition is assumed at the chamber and conduit walls, that is, $\mathbf{u} = \dot{\mathbf{d}}$ at the fluid-structure interface Γ_{FS} (see equations (7) and (15)) and $\mathbf{u} = \mathbf{0}$ along the rest of the walls. The horizontal component of the velocity is set to zero along the symmetry axis. Pressure at the computational outlet is fixed to lithostatic. A major inconvenience of cutting the conduit is that the outflow boundary condition becomes a time-dependent unknown of the problem and some approximate boundary condition must be used. The adoption of the lithostatic value can be justified as a first approximation to this unknown value because the average stress field within the conduit can not be far from lithostatic if the conduit is to remain open against compression of the host rocks. In the simulation described, the assumed mean density of the host rock is ρ_r =2600kg m^{-3}, implying a pressure of 90 MPa at the outlet. Initial values are assigned to velocity and pressure. Magma is assumed to be at rest before the eruption. The initial pressure distribution is assumed to be magmastatic. The chamber is filled with rhyolitic magma of density ρ_l =2400 kg m^{-3}, temperature T =850°C, viscosity μ =10^4 Pa s, and a constant water content of W =0.0425 (4.25 wt%). Under these conditions the exsolution level is located initially 200 m below the chamber roof, and 23% of the chamber volume is initially vesiculated. Driving the eruption is the density contrast between magma and the subsiding block, which induces downward movement of the block and squeezes magma out of the chamber through the ring fault [see *Gudmundsson*, 1998; *Martí et al.*, 2000].

The subsidence of the block versus time is shown in Figure 6. From this it can be seen that as soon as caldera collapse begins, the downward velocity of the subsiding block increases rapidly due to buoyancy effects. However, viscous forces, as well as the pressure exerted by the magma on the block, rapidly compensate for the density differences, making the net force acting on the block nearly zero. The result is that the block subsides at an approximately constant velocity, here of 0.55 m/s. This nearly constant velocity is maintained throughout the eruptive process, ending only during the last phase of the eruption, when the block begins to slow before impacting on the bottom of the chamber. A consequence of this is that the eruption rate rapidly increases to a plateau value with a final, relatively sudden, decrease (Figure 7). This numerical result is in excellent qualitative agreement with intensities inferred for caldera-forming eruptions [*Smith*, 1979; *Martí et al.*, 2000].

Figure 4. General and detailed views of the first and the last finite element method (FEM) meshes used in computations. Meshes are made of with triangular linear elements and, on average, have 10,000 nodal points. Although only two meshes are shown in the figure, the whole simulation requires up to six different meshes for the fluid (i.e., five remeshings).

The variation of erupted mass versus time (Figure 8) is estimated by computing the integral

$$\int_0^{T_{fin}} \left(\oint_{S_c} \rho \mathbf{u} \cdot \mathbf{n} \, dS \right) dt \quad , \tag{17}$$

where S_c is the section of the conduit (of the ring fault) and T_{fin} is the final time of analysis. The simulations suggest that once caldera collapse has started, it will tend to empty most of the chamber. However, note that in the simulations the end of the eruption is prescribed by the geometrical criteria of the subsiding block impacting on the bottom of the chamber, in this case 475 m of subsidence. This represents an extreme case, but not unrealistic, where the subsidence is the maximum allowed, most of the magma is extruded, and the original magma chamber is destroyed. In natural systems the process may stop earlier for two main reasons. First, the chamber may well be chemically heterogeneous. Magma at the base of the chamber of density exceeding that of the subsiding block would result in

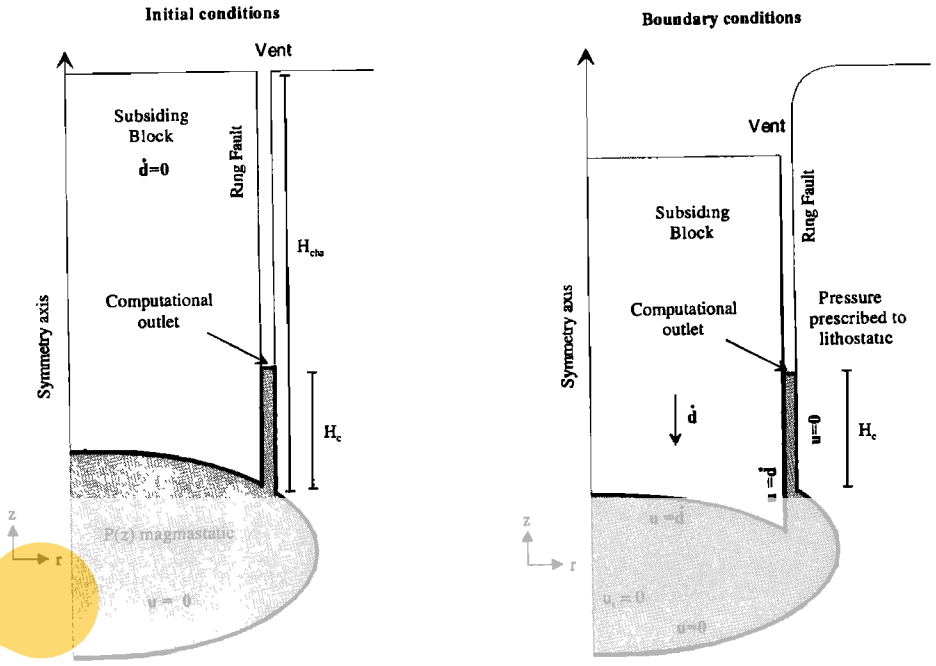

Figure 5. Schematic of boundary and initial conditions.

withdrawal of only the uppermost parts of the chamber filled with lighter magma. In fact, field evidence shows that in many cases, caldera-forming eruptions end with the emplacement of nonvesicular silicic lava domes along the ring fault [*Walker*, 1984; *Lipman*, 1984, 1997; *Martí et al.*, 2000]. Another possible stop to the process could be a closure of the conduit caused by a change in the local stress field or by a nonverticality of the ring fault fissure. The existence of inward dipping ring faults [*Walker*, 1984; *Lipman*, 1997] could result rapidly in closure of the fault due to subsidence of the block.

Figures 9 and 10 show density contours and streamlines at different time instants. A characteristic feature of the simulations is that the exsolution level moves downward with a velocity similar to the subsiding block. This is also illustrated in Figure 11, where the position of the exsolution level along the axis of symmetry is plotted versus time. A feature of the simulations is that the exsolution surface is not horizontal because subsidence produces a lateral pressure gradient. Pressure is greater below the top center of the chamber and lower at the outermost part, below the conduit entrance (Figure

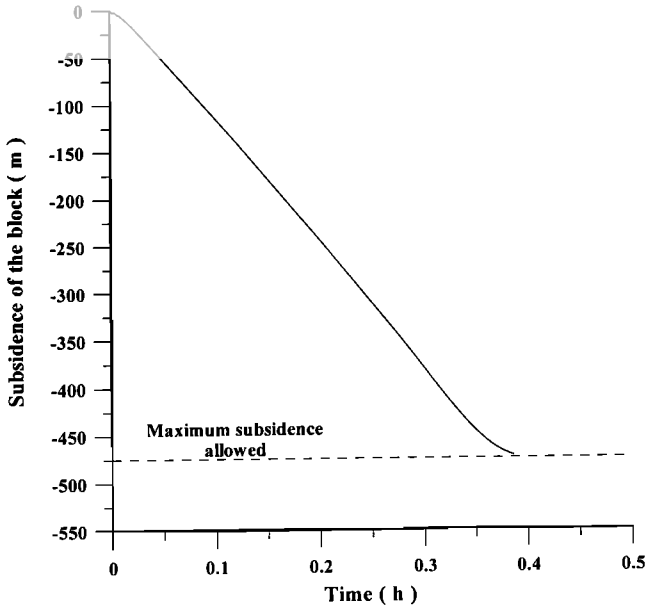

Figure 6. Subsidence of the collapsing block (in meters) plotted versus time (in hours). Note how the slope of the curve is, during most of the process, approximately constant. It corresponds to the phase of constant terminal velocity. The maximum subsidence allowed (by geometrical considerations) is indicated by the dashed line.

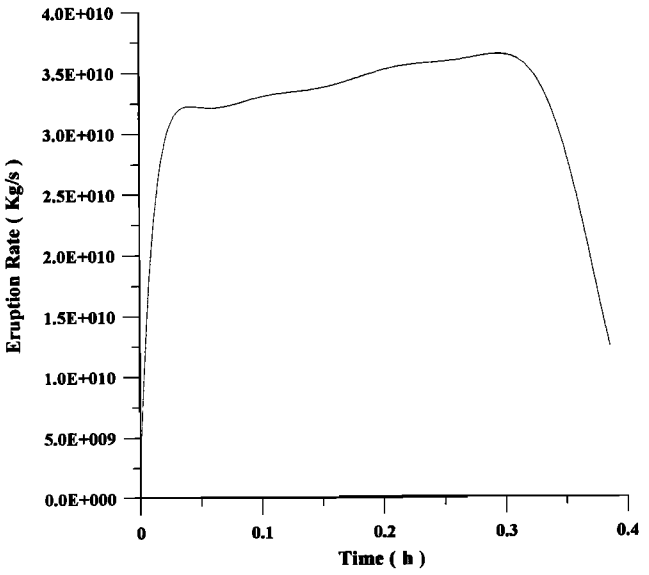

Figure 7. Eruption rate (in kilograms per second) versus time (in hours). A consequence of the kinematic behavior of the subsiding block is that the eruption rate remains approximately constant during most of the eruption (plateau phase).

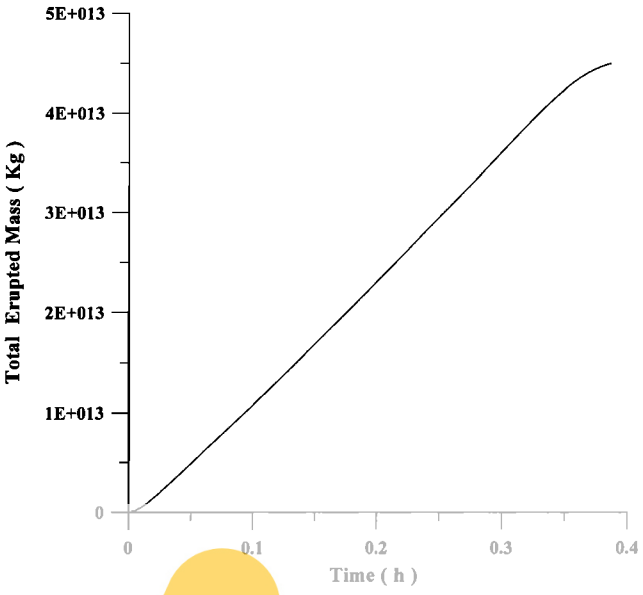

Figure 8. Total erupted mass (in kilograms) versus time (in hours).

10). Owing to the pressure dependence of volatile solubility, this phenomenon has a dramatic effect, tending to concentrate volatiles exsolution in the region below the ring fault. This is consistent with recent analytical results [*Gudmundsson*, 1998; *Martí et al.*, 2000] and explains the driving mechanism for the eruption of large volumes of ignimbrites during caldera-forming eruptions.

As eruption proceeds, a major central vortex, and secondary small ones, may develop at the outermost part of the chamber, just below the conduit entrance. This development is illustrated in Figure 12, where streamlines around the conduit entrance are shown at four different time instants. The vortex arises because the no-slip condition at the fluid-structure interface induces a tangential slide. This kinematic behavior is similar to a driven cavity flow [*Ghia et al.*, 1982; *Shen*, 1991]. In the case of caldera-forming eruptions, numerical simulations suggest that the formation of vortices is plausible for relatively low-viscosity (10^3-10^4 Pa s) magmas (at moderate to high Reynolds numbers). This could have important petrologic implications because vortices might explain magma mingling and mixing of a chemically stratified magma chamber. Many explosive, caldera-forming eruptions are characterized by magma mixing in their ignimbrite products [*Hildreth*, 1981; *Lipman*, 1984; *Henry et al.*, 1988].

Some results of the numerical simulations, such as subsidence velocity, eruption rate, or vortex formation, are strongly dependent on magma viscosity. To investigate this dependency, simulations considering different magma viscosities of 10^3, 10^4, and 10^5 Pa s have been performed. Figure 13 shows how the vortex formation is impeded if the magma is viscous enough, that is, if the Reynolds number of the problem is low. As expected, the higher the magma viscosity, the lower is the terminal subsidence velocity and the longer the eruption lasts. It should be noted that all simulations underestimate the force acting over the falling block due to the cutting of the computational domain. The viscous contribution at the uppermost part of the conduit, where magma viscosity increases notably due to volatile exsolution, would lead to a lower terminal velocity and hence to a longer eruption. While the results obtained here are still applicable, in the real case a much longer timescale would probably be observed.

5. Summary and Conclusions

A procedure to solve the Navier-Stokes equations with mechanical coupling has been developed and implemented using a finite element method and applied to determine the

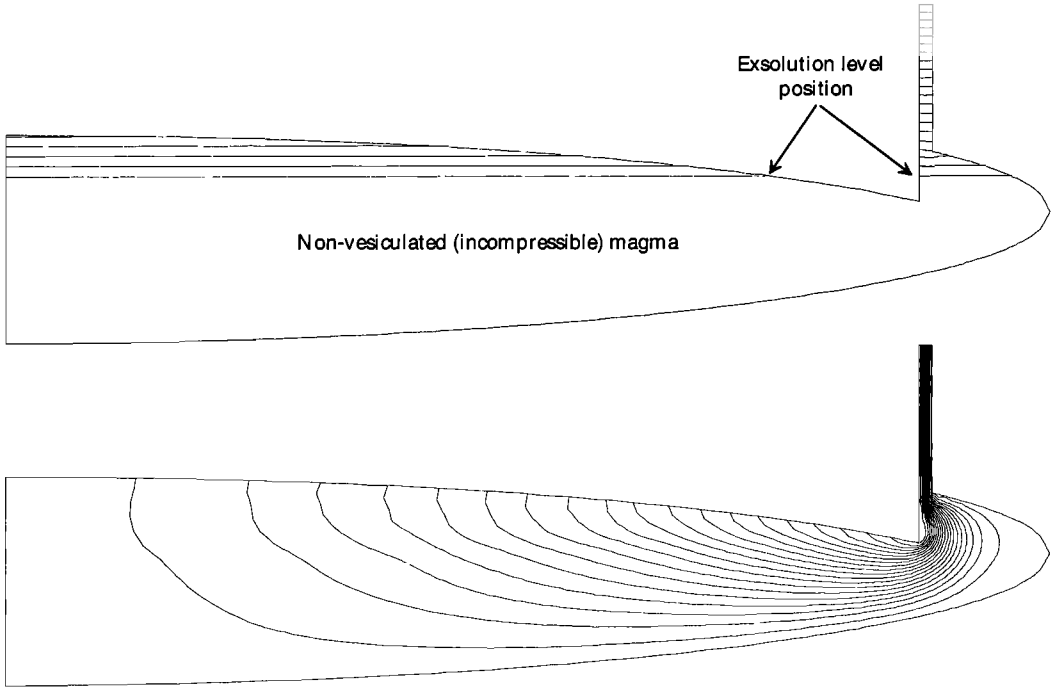

Figure 9. Results at t =10 min. (top) Contours of density. The position of the exsolution level determines the transition between the incompressible and the compressible regimes. (bottom) Streamlines.

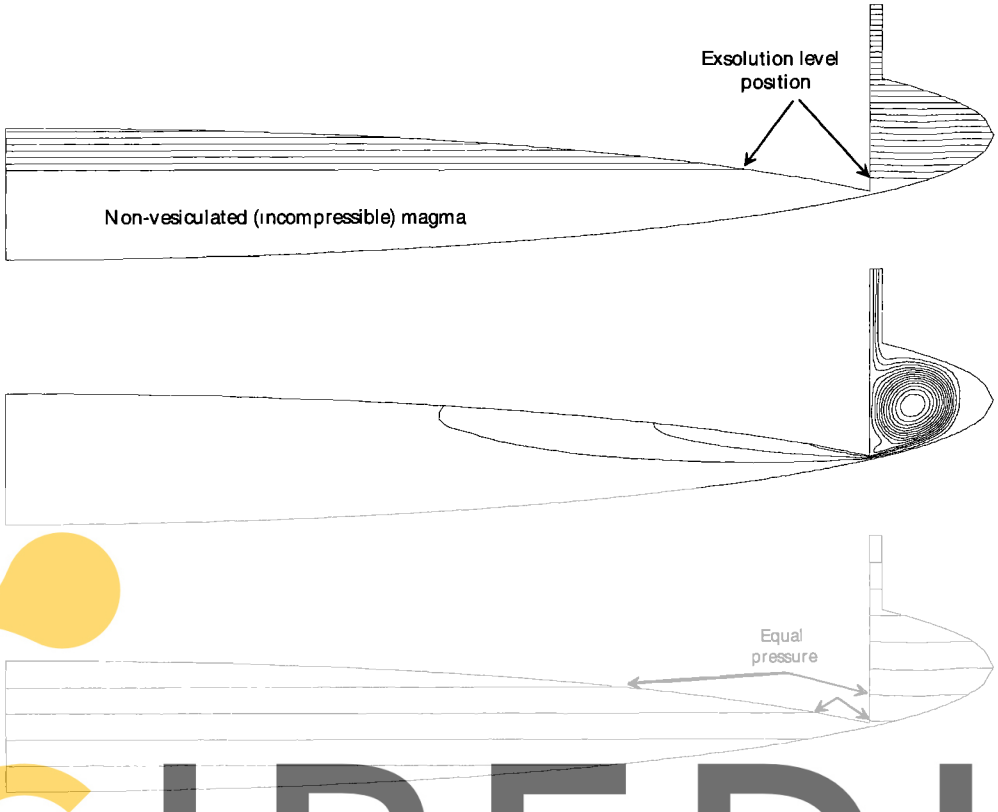

Figure 10. Results at t =22.5 min. (top) Contours of density, (middle) Streamlines. (bottom) Contours of pressure. Note how the pressure below the block (below the roof of the chamber) is greater than at the entrance of the conduit. Since volatile solubility depends on pressure, it induces a major exsolution of volatiles just below the ring fault.

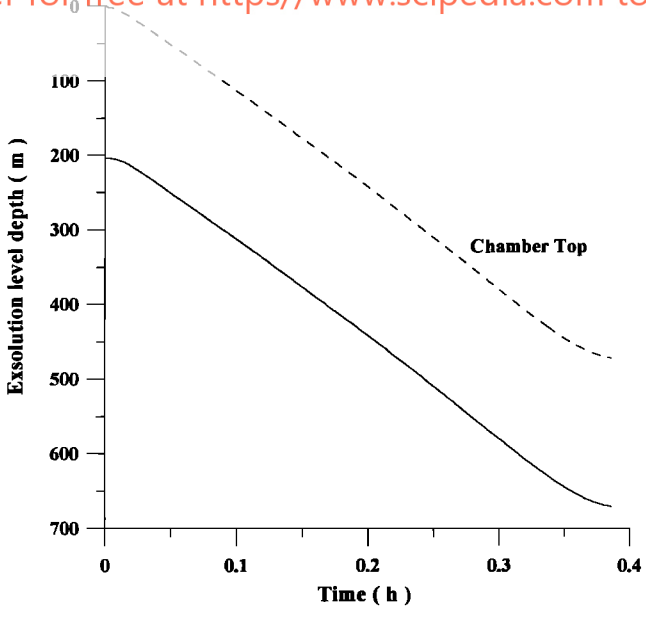

Figure 11. Position of the exsolution level (in meters) along the symmetry axis plotted versus time. The origin of coordinates is the position of the chamber top at t =0. The (variable) position of the chamber top is also indicated by a dashed line. Note how the exsolution level shifts downward with a velocity similar to that of the subsiding block.

dynamics of magma withdrawal from crustal reservoirs during explosive, caldera-forming eruptions. The Navier-Stokes equations are considered in the frame of an arbitrary Lagrangian-Eulerian (ALE) formulation that is especially suitable for fluid-structure interaction problems. This coupled problem is solved by means of a staggered procedure where the fluid and the structural equations are alternately integrated in time with separate solvers.

Natural systems are extremely complex and involve many variables difficult to measure or poorly constrained. Therefore a physical model, including some necessary assumptions and a state law for the magmatic mixture under the homogeneous approach (bubbly flow regime), has been proposed. As such, predictions of the model should be viewed with caution and regarded as a support to traditional geological, geophysical, and geochemical approaches. Different simulations of a wide variety of possibilities have been performed.

Numerical results provide insights into the caldera-forming processes that help improve our understanding of magma withdrawal dynamics during such explosive eruptions, refining the interpretation of the caldera products. The main numerical results and their geological interpretations can be summarized as follows:

1. During caldera-forming eruptions the velocity of the subsiding block increases rapidly to a constant value, which depends strongly on magma viscosity.

2. The eruption rate increases rapidly at the beginning of caldera subsidence, a plateau phase corresponds to the steady

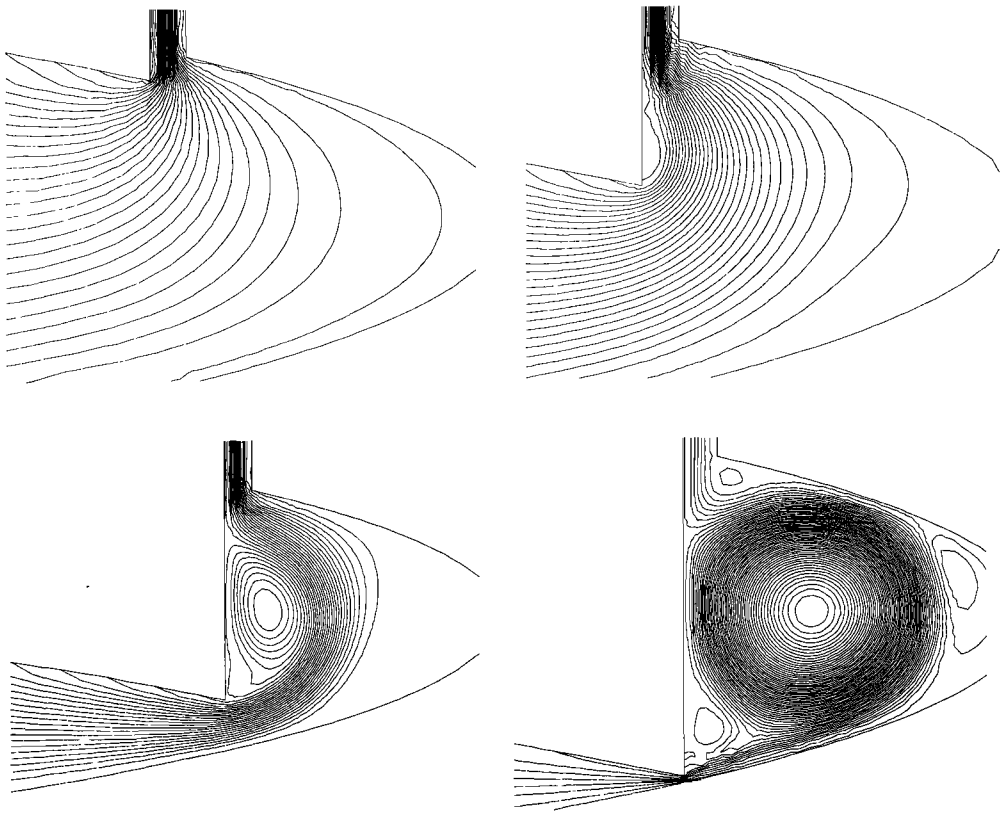

Figure 12. Zoom of the streamlines at the rightmost part of the chamber, below the entrance of the conduit. This figure illustrates the development of a large central vortex as the eruption proceeds. The corresponding time instants are (top left) t =2 min, (top right) t =7 min, (bottom left) t =12 min, and (bottom right) t =16 min. Pictures are not on the same scale.

fall velocity, and, finally, a sudden decrease is observed. These phases correspond to the initiation of collapse and enlargement of the ring fault, the main ignimbrite phase, and the cessation of explosive activity and emplacement of degassed magma into the ring fault, respectively.

3. Once initiated, the process of collapse stops when most of the chamber has been emptied, in the case of homogeneous chambers, or when most of the silicic, volatile-rich magma has been erupted, in the case of zoned chambers. Structural and geometrical effects (i.e., the ring fault geometry) may also influence the cessation of the caldera subsidence.

4. Depending on magma viscosity, a vortex may develop at the external parts of the chamber, beneath the ring fault. This phenomenon is likely to occur if magma viscosity is low and may generate mingling and mixing of magmas initially located at different depths.

5. The exsolution level deepens with a velocity similar to that of the subsiding block. However, the exsolution surface is not horizontal because the movement of the block causes a lateral pressure gradient. Most exsolution takes place below the ring fault. This suggests that volatiles exsolution is an efficient mechanism to sustain such eruptions, and to explain the production of large volumes of ignimbrites.

The simple model presented offers the first comprehensive approach to magma withdrawal dynamics during explosive, caldera-forming eruptions. We have described the mathematical method used to calculate the physical model. Future studies should include temperature dependencies, variable magma viscosity, chemical heterogeneities, and coupling with the dynamics of the conduit, in order to improve our knowledge of the most violent volcanic eruptions that can occur on the Earth's surface.

Notation

a major axis of the elliptical magma chamber.
a_r distance between the ring fault and the symmetry axis.
A^e area of an element of the FEM mesh.
b minor axis of the elliptical magma chamber.
$\mathbf{d}$ position of the structure (of the subsiding block).
$\dot{\mathbf{d}}$ velocity of the structure (of the subsiding block).
$\ddot{\mathbf{d}}$ acceleration of the structure (of the subsiding block).
$\mathbf{f}^{FS}$ force exerted by the fluid over the structure.
$\mathbf{g}$ gravity acceleration.
H_c computational height of the volcanic conduit.
H_{cha} depth of the magma chamber.
m parameter of the Henry solubility law.
M_b mass of the subsiding block.
$\mathbf{n}$ outward unit normal.
p pressure.
p_e critical (exsolution) pressure.
Q perfect gas constant.
r_r thickness of the ring fault.
s parameter of the Henry solubility law.
S_c section of the volcanic conduit (of the ring fault).
t time.

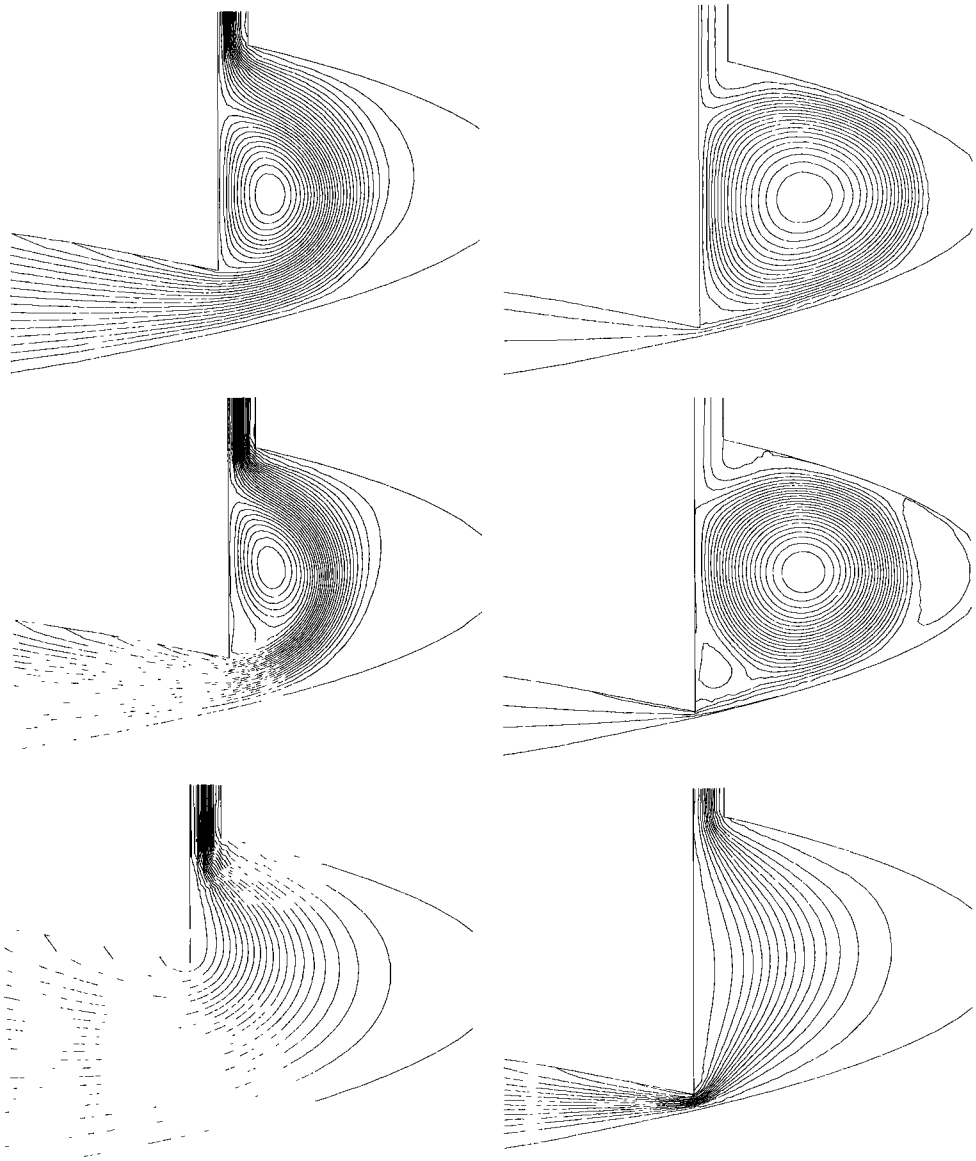

Figure 13. Zoom of the streamlines below the entrance of the conduit. Results are for magma viscosities of (top) 10^3 Pa s, (middle) 10^4 Pa s, and (bottom) 10^5 Pa s. Assuming that $\dot{\mathbf{d}}$ is 0.5 m s^{-1}, the corresponding Reynolds numbers are 60, 6, and 0.6 respectively. The cases with viscosities 10^3 Pa s and 10^4 Pa s are very similar. However, no vortex is formed when the viscosity is 10^5 Pa s.

T temperature.
$\mathbf{u}$ velocity of the fluid (magma).
$\mathbf{U}$ momentum of the fluid (magma).
$\hat{\mathbf{u}}$ velocity of the ALE dynamic mesh.
W volatile mass fraction.
$\hat{\mathbf{x}}$ position (coordinates) of the ALE dynamic mesh.
χ solubility.
Δt time step size.
Γ_{FS} fluid-structure interface.
μ viscosity.
ρ density of the magmatic mixture.
ρ_l density of the liquid.
ρ_r averaged density of host rock.
Ω_F domain of the fluid.
ξ function of the quasi-Laplacian method.

Acknowledgments. This research has been supported (in part) by the EC contract ENV4-CT96-0259 and the CICYT project AMB96-0498-C04. A.F. is grateful for a CIRIT research fellowship. G. Ablay revised the English text. We also thank two anonymous reviewers for their useful comments.

References

Blom, F.J., A monolithical fluid-structure interaction algorithm applied to the piston problem, *Comput. Methods Appl. Mech. Eng., 167*, 369-391, 1998.

Bower, S., and A.W. Woods, Control of magma volatile content and chamber depth on the mass erupted during explosive volcanic eruptions, *J. Geophys. Res., 102*, 10,273-10,290, 1997.

Branney, M.J., Downsag and extension at calderas: New perspectives on collapse geometries from ice-melt, mining and volcanic subsidence, *Bull. Volcanol., 57*, 303-318, 1995.

Druitt, T.H., and R.S.J. Sparks, On the formation of calderas during ignimbrite eruptions, *Nature, 310*, 679-681, 1984.

Farhat, C., M. Lesoinne, and N. Maman, Mixed explicit/implicit time integration of coupled aerolastic problems: Three-field formulation, geometric conservation and distributed solution, *Int. J. Numer. Methods Fluids, 21*, 807-835, 1995.

Folch, A., A numerical formulation to solve the ALE Navier-Stokes

equations applied to the withdrawal of magma chambers, *Ph.D. thesis*, Univ. Politèc. de Catalunya, Barcelona, Spain, 2000.

Folch, A., J. Marti, R. Codina, and M. Vázquez, A numerical model for temporal variations during explosive central vent eruptions, *J. Geophys. Res.*, *103*, 20,883-20,899, 1998.

Folch, A., M. Vázquez, R. Codina, and J. Martí, A fractional-step finite-element method for the Navier-Stokes equations applied to magma chamber withdrawal, *Comput. Geosci.*, *25*, 263-275, 1999.

Ghia, U., K.N. Ghia, and C.T. Shin, High-Re solutions for incompressible flow using the Navier-Stokes equations and a multigrid method, *J. Comput. Phys.*, *48*, 387-411, 1982.

Gudmundsson, A., The formation of collapse calderas, *Geology, 16*, 808-810, 1988.

Gudmundsson, A., Formation and development of normal-fault calderas and the initiation of large explosive eruptions, *Bull. Volcanol.*, *60*, 160-171, 1998.

Gudmundsson, A., J. Martí, and E. Turón, Stress fields generating ring faults in volcanoes, *Geophys. Res. Lett.*, *24*, 1559-1562, 1997.

Henry, C.D., J.G. Price, and R.C. Smith, Chemical and thermal zonation in a mild-alkaline magma system in Infiernito caldera, trans-pecos Texas, *Contrib. Mineral. Petrol.*, *98*, 194-211, 1988.

Hildreth, W., Gradients in silicic magma chambers: Implications for lithospheric magmas, *J. Geophys. Res.*, *86*, 10,153-10,192, 1981.

Houzeaux, G., and R. Codina, Transmission conditions with constraints in domain decomposition methods for flow problems, *Commun. Numer. Methods Eng.*, *17*, 179-190, 2001.

Hughes, T. J. R., W. K. Liu, and T. K. Zimmerman, Lagrangian-Eulerian finite element formulation for incompressible viscous flow, *Comput. Methods. Appl. Mech. Eng.*, *29*, 329-349, 1981.

Lipman, P.W., The roots of ash flow calderas in western North America: Windows into tops of granitic batholiths, *J. Geophys. Res* , *89*, 8801-8841, 1984.

Lipman, P.W., Subsidence of ash-flow calderas: Relation to caldera size and magma-chamber geometry, *Bull. Volcanol.*, *59*, 198-218, 1997.

Martí, J., G. Ablay, L.T. Redshaw, and R.S.J. Sparks, Experimental studies of collapse calderas, *J. Geol. Soc. London*, *151*, 919-929, 1994.

Martí, J., A. Folch, G. Macedonio, and A. Neri, Pressure evolution during caldera forming eruptions, *Earth Planet. Sci. Lett.*, *175*, 275-287, 2000.

Masud, A., and T.J.R. Hughes, A space-time Galerkin/least-squares finite element formulation of the Navier-Stokes equations for moving domain problems, *Comput. Methods Appl. Mech. Eng.*, *146*, 91-126, 1997.

McLeod, P., The role of magma buoyancy in caldera-forming eruptions, *Geophys. Res. Lett.*, *26*, 2299-2302, 1999.

Papale, P., Modeling of magma ascent along volcanic conduits: A review, in *The Mitigation of Volcanic Hazards, ECC Report*, pp. 5-40, Environ. Clim. programme, Luxemburg, 1996.

Roberts, J. L., The intrusion of magmas into brittle rocks, in *Mechanisms of igneous intrusion*, edited by G. Newall and N. Rast, pp. 287-338, Gallery Press, Liverpool, 1970.

Shen, J., Hopf bifurcation of the unsteady regularized driven cavity-flow, *J. Comput. Phys.*, *95*, 228-245, 1991.

Smith, R.L., Ash flow magmatism, *Spec. Pap. Geol. Soc. Am.*, *180*, 5-27, 1979.

Smith, R.L., and R.A. Bailey, Resurgent caulderons, *Mem. Geol. Soc. Am.*, *116*, 613-622, 1968.

Spera, F., Some numerical experiments on the withdrawal of magma from crustal reservoirs, *J. Geophys. Res.*, *89*, 8222-8236, 1984.

Tait, S., C. Jaupart, and S. Vergniolle, Pressure, gas content and eruption periodicity of a shallow crystallizing magma chamber, *Earth Planet. Sci. Lett.*, *92*, 107-123, 1989.

Trial, A. F., F. Spera, J. Greer, and D. Yuen, Simulations of magma withdrawal from compositionally zoned bodies, *J. Geophys. Res.*, 97, 6713-6733, 1992.

Walker, G.P.L., Downsag calderas, ring faults, caldera sizes, and incremetnal growth, *J. Geophys. Res.*, *89*, 8407-8416, 1984.

Williams, H., Calderas and their origin, Bull. Univ. of Calif., Dep. of Geol. Sci., *25*, pp. 239-346, 1941.

Willams, H., and A.R. McBirney, in *Volcanology*, 397 pp., Freeman Couper and Co., San Francisco, Calif., 1979.

Wohletz, K.H., T.R. McGetchin, M.T. Standford II, and E.M. Jones, Hydrodynamic aspects of caldera-forming eruptions: numerical models, *J. Geophys. Res* , *89*, 8269-8285, 1984.

R. Codina and A. Folch, International Center for Numerical Methods in Engineering, Universitat Politècnica de Catalunya, c/ Jordi Girona 1-3, Edifici C1, 08034 Barcelona, Spain. (codina@upc.es; folch@cimne.upc.es).

J. Martí, Laboratory of Simulation of Geological Processes, Institute of Earth Sciences "Jaume Almera," /Lluís Solé Savarís s/n, 08028 Barcelona, Spain. (joan.marti@ija.csic.es).

(Received July 17, 2000; revised January 22, 2001;
accepted February 22, 2001.)